Russian Journal of Earth Sciences

Linear Perturbations of the Bloch Type of Space-Periodic Magnetohydrodynamic Steady States. II. Numerical Results

R. Chertovskih[*,1] **and V. Zheligovsky**[2]

[1]SYSTEC, ARISE, Faculty of Engineering, University of Porto, Porto, Portugal
[2]Institute of Earthquake Prediction Theory and Mathematical Geophysics RAS, Moscow, Russian Federation
* **Correspondence to:** V. Zheligovsky, vlad@mitp.ru

Abstract: We consider Bloch eigenmodes of three linear stability problems: the kinematic dynamo problem, the hydrodynamic and MHD stability problem for steady space-periodic flows and MHD states comprised of randomly generated Fourier coefficients and having energy spectra of three types: exponentially decaying, Kolmogorov with a cut off, or involving a small number of harmonics ("big eddies"). A Bloch mode is a product of a field of the same periodicity as the perturbed state and a planar harmonic wave, $\exp(i\mathbf{q}\cdot\mathbf{x})$. Such a mode is characterized by the ratio of spatial scales which, for simplicity, we identify with the length $|\mathbf{q}| < 1$ of the Bloch wave vector $\mathbf{q}$. Computations have revealed that the Bloch modes, whose growth rates are maximum over $\mathbf{q}$, feature the scale ratio that decreases on increasing the nondimensionalized molecular diffusivity and/or viscosity from 0.03 to 0.3, and the scale separation is high (i.e., $|\mathbf{q}|$ is small) only for large molecular diffusivities. Largely this conclusion holds for all the three stability problems and all the three energy spectra types under consideration. Thus, in a natural MHD system not affected by strong diffusion, a given scale range gives rise to perturbations involving only moderately larger spatial scales (i.e., $|\mathbf{q}|$ only moderately small), and the MHD evolution consists of a cascade of processes, each generating a slightly larger spatial scale; flows or magnetic fields characterized by a high scale separation are not produced. This cascade is unlikely to be amenable to a linear description. Consequently, our results question the allegedly high role of the α-effect and eddy diffusivity that are based on spatial scale separation, as the primary instability or magnetic field generating mechanisms in astrophysical applications. The Braginskii magnetic α-effect in a weakly non-axisymmetric flow, often used for explanation of the solar and geodynamo, is advantageous not being upset by a similar deficiency.

Keywords: Kinematic dynamo problem, hydrodynamic linear stability problem, magnetohydrodynamic linear stability problem, Bloch mode, magnetic α-effect, AKA-effect, combined magnetohydrodynamic α-effect, magnetic eddy diffusivity, eddy viscosity, scale separation, pseudospectral methods.

Citation: Chertovskih, R., and V. Zheligovsky (2023), Linear Perturbations of the Bloch Type of Space-Periodic Magnetohydrodynamic Steady States. II. Numerical Results, *Russ. J. Earth. Sci.*, 23, ES4004, https://doi.org/10.2205/2023es000838

Research Article

Received: 22 November 2022
Accepted: 7 March 2023
Published: 22 October 2023

1. Introduction

In order to investigate the physical realizability of the α-effect and eddy diffusivity based on spatial scale separation, we consider here numerically Bloch eigenmodes in three linear stability problems: the kinematic dynamo problem, the hydrodynamic and MHD stability problem for steady space-periodic flows and MHD states. This paper is a direct continuation of [*Chertovskih and Zheligovsky*, 2023], where we have reviewed the literature and considered in detail the philosophy behind our project, the equations describing the stability problems, and the mathematical results and numerical tools that can be employed for tackling them (see also [*Zheligovsky*, 2011]).

The following question is crucial for assessing the feasibility of the action of the α-effects and eddy diffusivities of various kinds (the magnetic, kinetic and combined

MHD ones), relying on the spatial scale separation in the natural hydromagnetic dynamos (foremostly, the astrophysical ones): is a significant scale separation stable and preserved during the temporal evolution of the dynamo, or is it unsustainable and destroyed by an inherent instability?

We focus on the small-scale turbulent motion of incompressible fluid and, in the MHD stability problem, on magnetic field, that are characterized by a certain range of spatial scales. For the sake of simplicity, the flow velocity and magnetic field are assumed to be space-periodic (with the periodicity cell $\mathbb{T}^3 = [-\pi,\pi]^3$) and steady. The direct and inverse energy cascades along the hierarchy of scales are supposed to give rise to a forcing supporting the steady states. The chosen characteristic scale is used in the definition of the nondimensionalized values of the diffusivity parameters, giving an opportunity to consider just limited intervals of their variation. We study multiscale (actually, two-scale) perturbations of the Bloch type that are products of a vector field of the same periodicity as the perturbed state and a planar harmonic wave, $e^{i\mathbf{q}\cdot\mathbf{x}}$. The large-scale wave vector $\mathbf{q}$ is an arbitrary real-valued three-dimensional constant vector; its length controls the level of the spatial scale separation. As explained in [*Chertovskih and Zheligovsky*, 2023], it suffices for our purposes to seek the dominant (maximum) growth rate in the parallelepiped

$$\mathbb{Q} = \{\mathbf{q} \,|\, 0 \le q_1 \le 1/2, \quad -1/2 \le q_2 \le 1/2, \quad -1/2 \le q_3 \le 1/2\}.$$

The outer fluid container is supposed to be sufficiently large so that its boundaries do not affect the processes that we investigate.

Let us recall (see the detailed explanations in [*Chertovskih and Zheligovsky*, 2023]) that the stability problems under consideration then reduce to the eigenvalue problems for the operators

$$d : \mathbf{b} \mapsto \eta\Delta_{\mathbf{q}}\mathbf{b} + \nabla\times(\mathbf{V}\times\mathbf{b}) + i\mathbf{q}\times(\mathbf{V}\times\mathbf{b})$$

in the kinematic dynamo problem,

$$\mathscr{H}_{\mathbf{q}} : \mathbf{v} \mapsto \nu\Delta_{\mathbf{q}}\mathbf{v} + \mathscr{P}_{\mathbf{q}}\Big(\mathbf{v}\times(\nabla\times\mathbf{V}) + \mathbf{V}\times(\nabla\times\mathbf{v}) + i\mathbf{V}\times(\mathbf{q}\times\mathbf{v})\Big)$$

in the hydrodynamic stability problem, and

$$\begin{aligned}\mathscr{M}_{\mathbf{q}} : (\mathbf{v},\mathbf{b}) \mapsto \Big(&\nu\Delta_{\mathbf{q}}\mathbf{v} + \mathscr{P}_{\mathbf{q}}\Big(\mathbf{v}\times(\nabla\times\mathbf{V}) + \mathbf{V}\times(\nabla\times\mathbf{v}) + i\mathbf{V}\times(\mathbf{q}\times\mathbf{v})\\ &+ (\nabla\times\mathbf{b})\times\mathbf{B} + i(\mathbf{q}\times\mathbf{b})\times\mathbf{B} + (\nabla\times\mathbf{B})\times\mathbf{b}\Big),\\ &\eta\Delta_{\mathbf{q}}\mathbf{b} + \nabla\times(\mathbf{v}\times\mathbf{B} + \mathbf{V}\times\mathbf{b}) + i\mathbf{q}\times(\mathbf{v}\times\mathbf{B} + \mathbf{V}\times\mathbf{b})\Big)\end{aligned}$$

in the full MHD stability problem. Here

$$\Delta_{\mathbf{q}} : \mathbf{f} \mapsto \nabla^2\mathbf{f} + 2i(\mathbf{q}\cdot\nabla)\mathbf{f} - |\mathbf{q}|^2\mathbf{f}$$

is the modified Laplacian, $\mathscr{P}_{\mathbf{q}}$ is the projector onto the space of three-dimensional space-periodic (with the periodicity cell $\mathbb{T}^3 = [-\pi,\pi]^3$) vector fields $\mathbf{f}$ such that $e^{i\mathbf{q}\cdot\mathbf{x}}\mathbf{f}$ is a solenoidal field, $\mathbf{V},\mathbf{B}$ the nondimensionalized flow and magnetic field that are subjected to the perturbations, η and ν are the nondimensionalized molecular magnetic diffusivity and viscosity, respectively. The eigenfunctions $(\mathbf{v},\mathbf{b})$ and $(\mathbf{v}^*,\mathbf{b}^*)$ associated with the *dominant* eigenvalues (having the maximum real part for a given $\mathbf{q}$, ν and η) have been computed employing the standard pseudospectral techniques by the code [*Zheligovsky*, 1993].

For reader's convenience, we now remind the notation introduced in [*Chertovskih and Zheligovsky*, 2023]. We denote by $\gamma^{\mathbf{b}}$, $\gamma^{\mathbf{v}}$ and $\gamma^{\mathbf{vb}}$ the maximum, over the wave vectors $\mathbf{q}$, growth rates of the generated magnetic field and perturbations in the kinematic dynamo, hydrodynamic and MHD linear stability problems, respectively. For a small scale ratio

$|\mathbf{q}| = \varepsilon$, the stability eigenmodes and the associated eigenvalues of the respective operator of linearization can be expanded in power series in this parameter:

$$\mathbf{v} = \sum_{n=0}^{\infty} \mathbf{v}_n(\mathbf{x}, \mathbf{X})\varepsilon^n, \qquad \mathbf{b} = \sum_{n=0}^{\infty} \mathbf{b}_n(\mathbf{x}, \mathbf{X})\varepsilon^n, \qquad \lambda = \sum_{n=0}^{\infty} \lambda_n \varepsilon^n. \tag{1}$$

The α-effect becomes a predominant instability mechanism based on scale separation, if $\lambda_0 = 0$. The mean eigenfields are then eigenfunctions of the α-effect operator (see [*Chertovskih and Zheligovsky*, 2023; *Zheligovsky*, 2011]); they evolve in the slow $O(\varepsilon)$ time scale. We denote by $\gamma_\alpha^{\mathbf{b}}$, $\gamma_\alpha^{\mathbf{v}}$ and $\gamma_\alpha^{\mathbf{vb}}$ the maximum slow-time growth rate of perturbations due to the action of the α-effect. These values are defined as $\max_{\mathbf{q}} \operatorname{Re} \lambda_1$; here λ_1 is the coefficient of the leading term in the expansion (1) of the eigenvalue λ for the respective problem. When the MHD steady state experiencing a perturbation is parity-invariant (i.e., satisfies $\mathbf{V}(\mathbf{x}) = -\mathbf{V}(-\mathbf{x})$ and $\mathbf{B}(\mathbf{x}) = -\mathbf{B}(-\mathbf{x})$), then the α-effect disappears (the α-effect tensor vanishes). When $\lambda_0 = \lambda_1 = 0$, the predominant instability mechanism based on scale separation is eddy diffusivity (in particular, eddy viscosity in the context of the hydrodynamic stability problem), aka the β-effect in the speak of the mean-field magnetohydrodynamics (see [*Krause and Radler*, 1980]). The mean stability eigenfield is then an eigenfunction of the eddy diffusivity operator (see [*Chertovskih and Zheligovsky*, 2023; *Zheligovsky*, 2011]). It evolves in the slow $O(\varepsilon^2)$ time scale, and we denote by $\gamma_{\mathrm{e}}^{\mathbf{b}}$, $\gamma_{\mathrm{e}}^{\mathbf{v}}$ and $\gamma_{\mathrm{e}}^{\mathbf{vb}}$ the maximum slow-time growth rate of perturbations due to the action of the eddy diffusivity. (Here and in the analogous notation for the α-effect case, superscripts refer to the three respective stability problems.) These values are defined as $\max_{\mathbf{q}} \operatorname{Re} \lambda_2$; here λ_2 is the coefficient of the leading term in the series (1) for the eigenvalue λ.

In section 2 we discuss how sample MHD steady states, whose perturbations we explore, have been generated. As mentioned above, we have carried out computations of the dominant growth rates of perturbations in the three linear stability problems. For each problem, we have generated sample steady states featuring different energy spectrum decay types: a steep exponential decay, the Kolmogorov spectrum with a cut off, and fields comprised of a small number of harmonics. Furthermore, for each problem and energy decay type, we made computations for non-symmetric steady states (possessing the α-effect) and for parity-invariant ones (possessing eddy diffusivity). We have thus considered 18 in total sample steady states. We discuss the observed behavior in section 3. Our conclusions are summarized in the last section.

2. Sample MHD steady states

In order to investigate numerically the instability mechanism under consideration, sample steady solenoidal $\mathbb{T}^3$-periodic fields $\mathbf{V}$ and $\mathbf{B}$ have been synthesized. The following procedure has been employed to construct generic flows or MHD states featuring the α-effect:

i) white-noise three-dimensional pseudo-random complex vectors $\mathbf{c_k}$ are seeded in the Fourier space on approximately a half of the regular grid (for $k_1 \geq 0$) of wave vectors $\mathbf{k}$;

ii) the condition $\mathbf{c_k} = \overline{\mathbf{c}}_{-\mathbf{k}}$ is used to initialize the remaining Fourier coefficients (so that the resultant field is real) and is imposed on the coefficients for $k_1 = 0$;

iii) the mean part is removed (setting $\mathbf{c}_0 = 0$) and the solenoidality condition (orthogonality of the Fourier coefficient to the respective wave vector, $\mathbf{c_k} \cdot \mathbf{k} = 0$) is enforced by removing the gradient part $(\mathbf{c_k} \cdot \mathbf{k})\mathbf{k}/|\mathbf{k}|^2$;

iv) depending on the desirable energy spectrum of the field, each coefficient $\mathbf{c_k}$ is divided by $4^{|\mathbf{k}|}$ (resulting in the exponential energy spectrum decay); $\mathbf{c_k}$ is divided by $|\mathbf{k}|^{11/6}$ when all wave numbers satisfy $|k_m| < 32$, or it is set to zero otherwise (the Kolmogorov spectrum with a cut off, see [*Frisch*, 1995]); or we set $\mathbf{c_k} = 0$ whenever $|k_m| > 2$ for at least one wave number (to obtain a field comprised of a relatively small number of harmonics);

v) finally, the field is normalized so that its r.m.s. value is equal to 1 (implying that $1/\nu$ can be regarded as the local Reynolds number and $1/\eta$ the local magnetic Reynolds number).

Such fields can be interpreted as building blocks in the viscous, inertial and large eddy subranges of spatial scales of turbulent flow or MHD state; we call them type V, I and E flows, respectively.

Sample parity-invariant fields have been synthesized by the same procedure with one exception: all the coefficients $\mathbf{c_k}$ generated and modified at the stages i) and ii) are imaginary.

3. Analysis of the behavior of the growth rates

We now present an overview of the numerical results obtained for the sample steady states. Figures 1–9 summarize the results of computations for the hydrodynamic stability problem, Figures 10–16 for the kinematic dynamo problem and Figures 17–23 for the MHD stability problem. All Figures 1–23, except for five Figures 3, 5, 8, 11 and 17, display in four panels how the results for individual sample steady states depend on the quantities parameterizing the linear stability problems (the horizontal axis is the molecular viscosity ν for the hydrodynamic stability problem, the molecular magnetic diffusivity η for the kinematic dynamo problem, or $\nu = \eta$ for the MHD linear stability problem). Panels (a) show graphs of the maximum (over the wave vectors $\mathbf{q}$ of the planar harmonic wave) growth rates, panels (b) the components and lengths of $\mathbf{q}$ for which the growth rates take these maximum values. Figures 1–4, 10–13 and 17–20 report numerical results for the generic sample states giving rise to the AKA-effect, magnetic and combined MHD α-effect, respectively. Panels (c) in these figures (except Figures 3, 11 and 17) show plots of the maximum (over the direction $\mathbf{l}$ of the wave vectors $\mathbf{q} = \varepsilon\mathbf{l}$) slow-time growth rate due to the action of the α-effect in the limit of infinitesimal spatial scale ratio $\varepsilon \to 0$ (see section 5.1 of *Chertovskih*

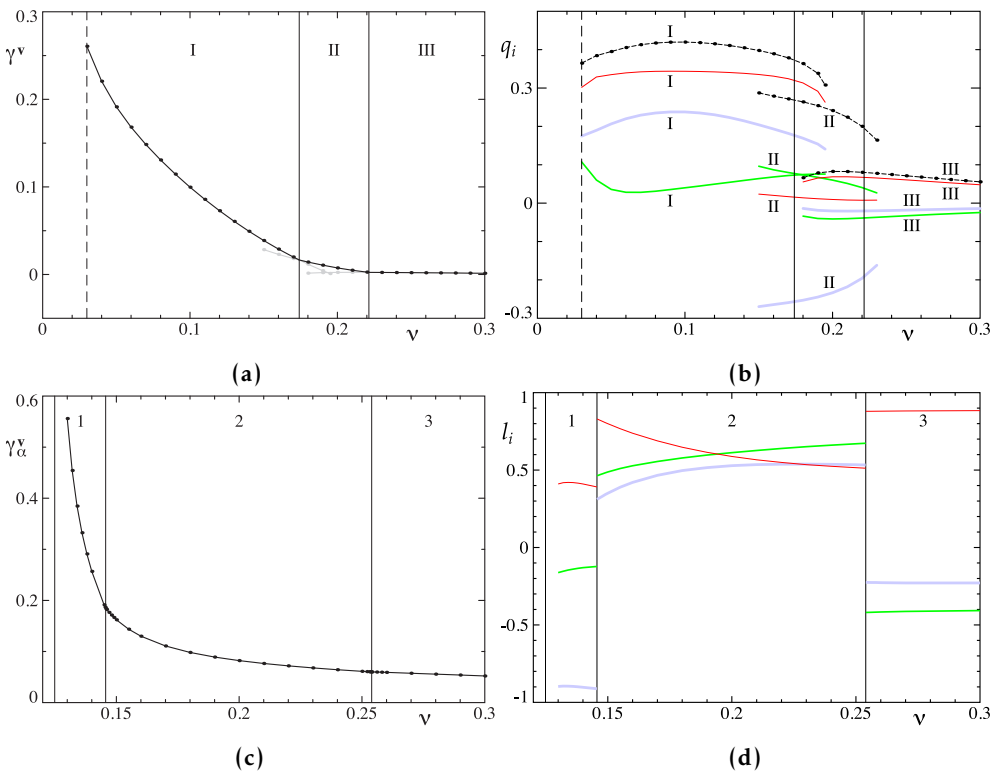

Figure 1. Maximum growth rates of the Bloch hydrodynamic linear stability modes (a) and maximum slow-time growth rates due to the action of the AKA-effect (c) for a sample non-parity-invariant steady flow of type V. Wave vectors $\mathbf{q}$ (b), for which the growth rates are shown in (a), and directions of the wave vectors (d), for which the growth rates are shown in (c).

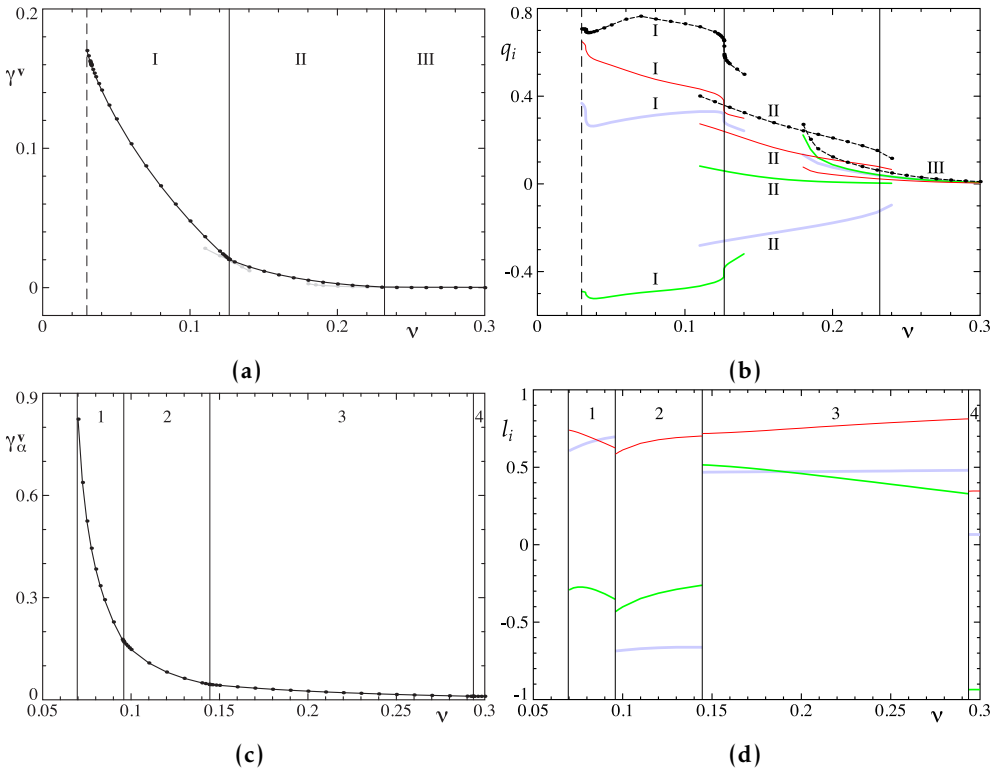

Figure 2. Same as in Figure 1, but for a sample non-parity-invariant flow of type I.

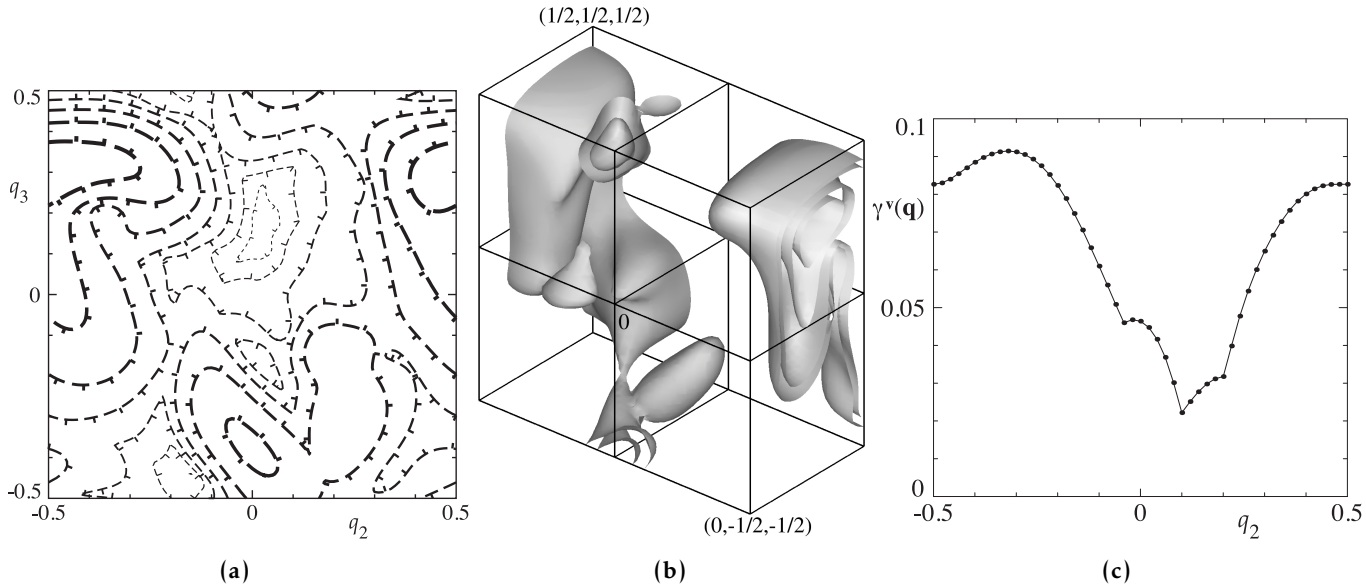

Figure 3. For $\nu = 0.1$, isolines of the dominant growth rates $\gamma^{\mathbf{v}}(\mathbf{q})$ of the Bloch hydrodynamic stability modes in the cross-section $q_1 = 0.32$ of the parallelepiped $\mathbb{Q}$ (a), isosurfaces of the growth rates (b) and the dominant growth rates as a function of q_2 on the line $q_1 = 0.48$, $q_3 = 0.3$ (c) for a sample non-parity-invariant flow of type E. The isolines are drawn for the growth rates that are integer multiples of 0.011 (the minimum and maximum $\gamma^{\mathbf{v}}$ in this plane are 0.0128 and 0.0950). The width of the isolines and dash length increase with the constant values along the curves. The isosurfaces are shown in $\mathbb{Q}$ at the levels of 75%, 80%, 90% and 95% of the maximum over $\mathbb{Q}$ value $\gamma^{\mathbf{v}}(\mathbf{q}) = 0.0951$ for $\mathbf{q} = (0.3110, 0.4967, 0.2967)$. The axis q_1 points inside $\mathbb{Q}$, the q_2 axis to the left, and the q_3 axis is vertical.

and Zheligovsky [2023]), i.e., the maximum real part of the leading term coefficient λ_1 in the expansion (1) of the growth rate λ in power series in ε. The remaining Figures 5–9, 14–16 and 21–23 present plots for the parity-invariant sample states lacking the α-effect, but giving rise to eddy viscosity, magnetic and combined MHD eddy diffusivity, respectively. Panels (c) in these figures (except Figures 5 and 8) show plots of the maximum (over the

directions $\mathbf{l}$ of the wave vectors $\mathbf{q} = \varepsilon\mathbf{l}$) slow-time growth rate due to the action of the respective large-scale eddy diffusivity in the limit $\varepsilon \to 0$, i.e., the maximum real part of the leading term coefficient λ_2 in the expansion (1) of λ. In all figures, panels (d) present the components of the unit vector $\mathbf{l}$ for which the growth rate shown in (c) is maximum. Bold dots in the graphs show the actually computed values. Finally, Figures 3, 5, 8, 11 and 17 illustrate the dependence of the dominant growth rate of the Bloch linear stability modes on the wave vector $\mathbf{q}$, e.g., show isosurfaces of λ in the wave vector domain $\mathbb{Q}$.

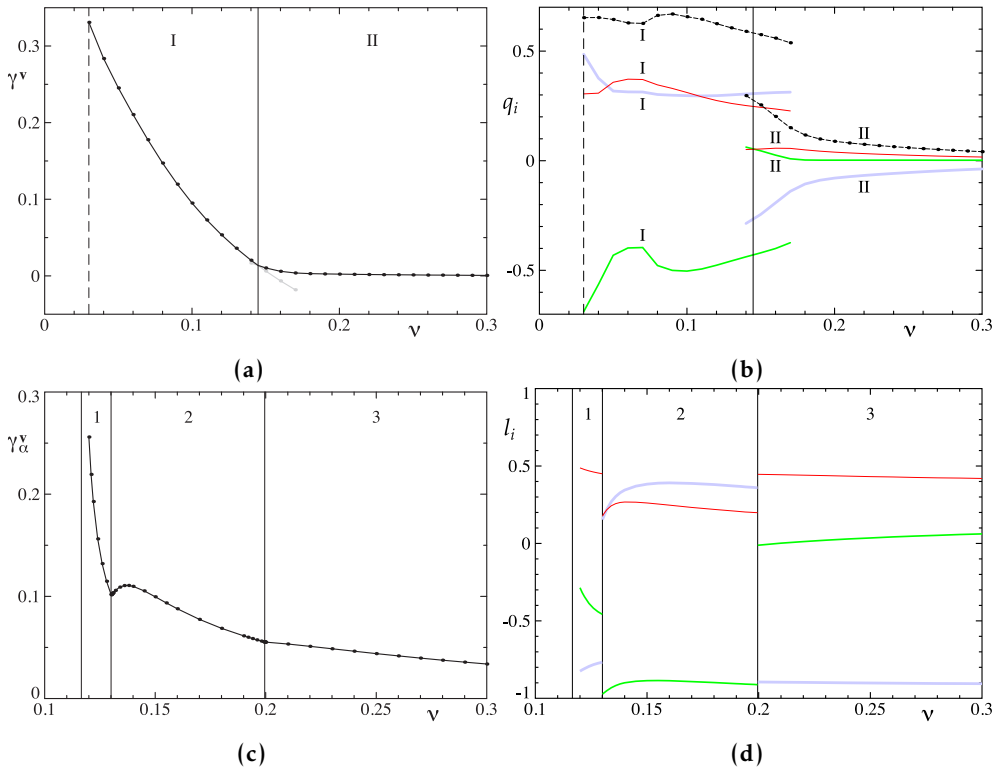

Figure 4. Same as in Figure 1, but for the sample non-parity-invariant flow of type E.

The globally maximum growth rates of linear perturbation modes have been computed in the ranges $0.03 \le \nu, \eta \le 0.3$. The maxima depend continuously on ν or η, and the associated stability modes constitute branches. In a branch, the dependencies of the modes and their growth rates on the parameter are smooth, as well as the dependence of the wave vector $\mathbf{q}$, for which the growth rate is maximum. We call "the interval of dominance of a branch" the interval of parameter values, where the growth rates of modes constituting the branch are globally maximum. In the plots of maximum growth rates and the respective $\mathbf{q}$ (panels (a) and (b) in Figures 1–23 except Figures 3, 5, 8, 11, 17), intervals of dominance of individual branches are delimited by thin vertical lines and the branches are numbered by Roman numerals. (The left boundary, $\nu = 0.03$ or $\eta = 0.03$, is shown by a thin dashed vertical line.) The molecular diffusivity range, for which we perform computations, splits in different problems into 2 to 6 intervals of dominance of distinct branches. Often branches can be extended outside their intervals of dominance by performing continuation in parameter; the modes, constituting extensions of the branches, still have locally maximum growth rates, which cease, however, to be global maxima. The growth rates of modes constituting extensions of the branches outside their intervals of dominance are shown in light gray in the plots in panels (a). We have checked that all such continuations involve local maxima by computing the Hessian of the growth rates. We have not intended to extend all branches, or to extend them on the largest possible diffusivity intervals.

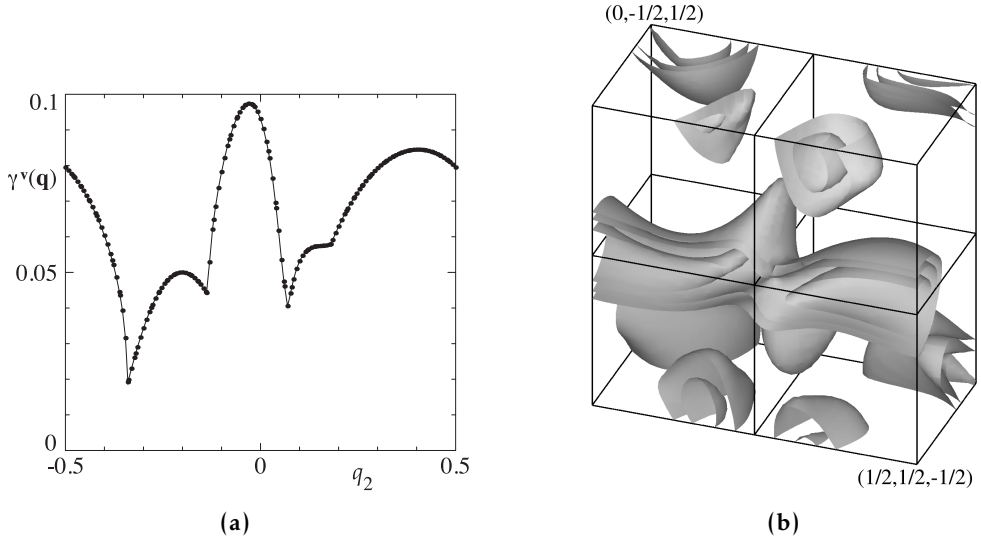

Figure 5. For $\nu = 0.1$, dominant growth rates $\gamma^{\mathbf{v}}(\mathbf{q})$ of the Bloch hydrodynamic stability modes as a function of q_2 on the line $q_1 = 0.44$, $q_3 = 0.16$ (a), and isosurfaces of the growth rates in $\mathbb{Q}$ at the levels of 70%, 80% and 90% of the maximum over $\mathbb{Q}$ value $\gamma^{\mathbf{v}}(\mathbf{q}) = 0.1283$ for $\mathbf{q} = (0.4615, 0.3878, 0.0175)$ (b) for a sample parity-invariant steady flow of type V. The axis q_1 points towards the reader, the frontal vertical plane is $q_1 = 1/2$, the q_2 axis points to the right, and the q_3 axis is vertical.

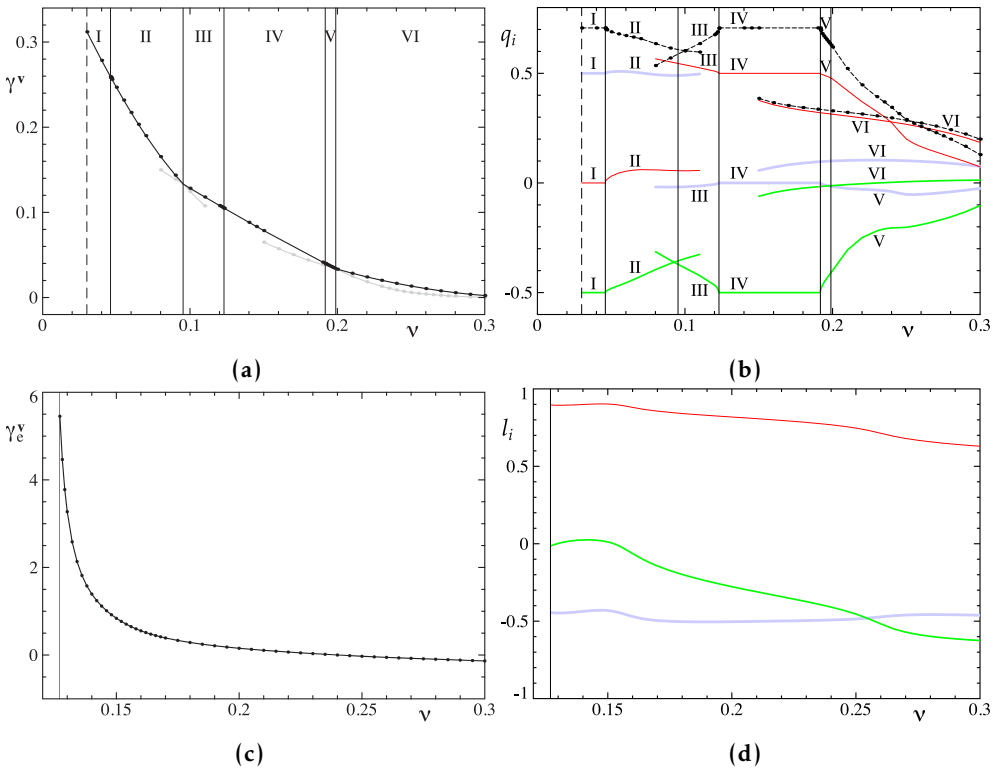

Figure 6. Panels (a), (b) and (d) same as in Figure 1a, 1b and 1d, but for the sample parity-invariant steady flow of type V, and maximum slow-time growth rates due to the action of the eddy viscosity Figure 1c. In intervals I and IV, the growth rates $\gamma^{\mathbf{v}}(\mathbf{q})$ are globally maximum over $\mathbb{Q}$ for $\mathbf{q} = (0, -1/2, 1/2)$ and $(1/2, -1/2, 0)$, respectively.

In panels (b) of all Figures except Figures 3, 5, 8, 11, 17, red, green and blue lines show the components q_1, q_2 and q_3, and black dashed lines show $|\mathbf{q}|$. (In order to demonstrate

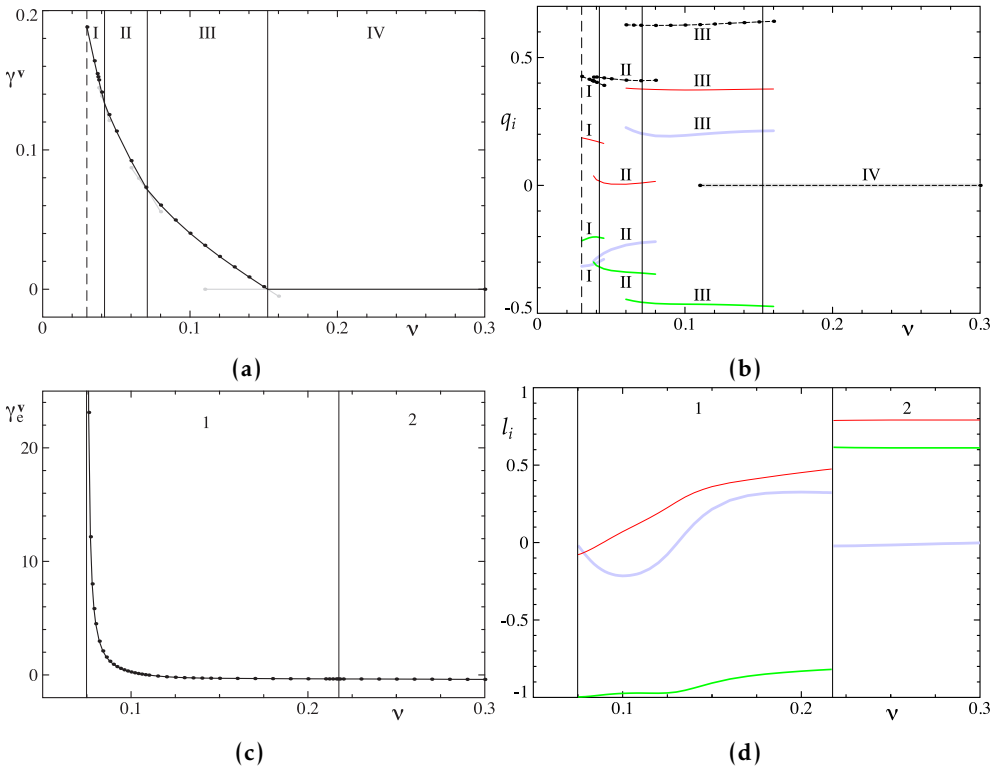

Figure 7. Same as Figure 6, but for a sample parity-invariant steady flow of type I. In interval IV, the globally maximum over $\mathbb{Q}$ growth rate is $\gamma^{\mathbf{v}}(\mathbf{q}) = 0$ for $\mathbf{q} = 0$.

that in each branch every q_i is a smooth function of the parameter ν or η, the selection criterion $\mathbf{q} \in \mathbb{Q}$ may be not enforced for a part of a graph of q_i.) Obviously, this color coding does not work, when all the three components are equal on an interval of the diffusive parameter; this does happen when the growth rates are globally maximum for half-integer wave vectors. The equal q_i's are then shown in panel (b) by a wide light gray line. We

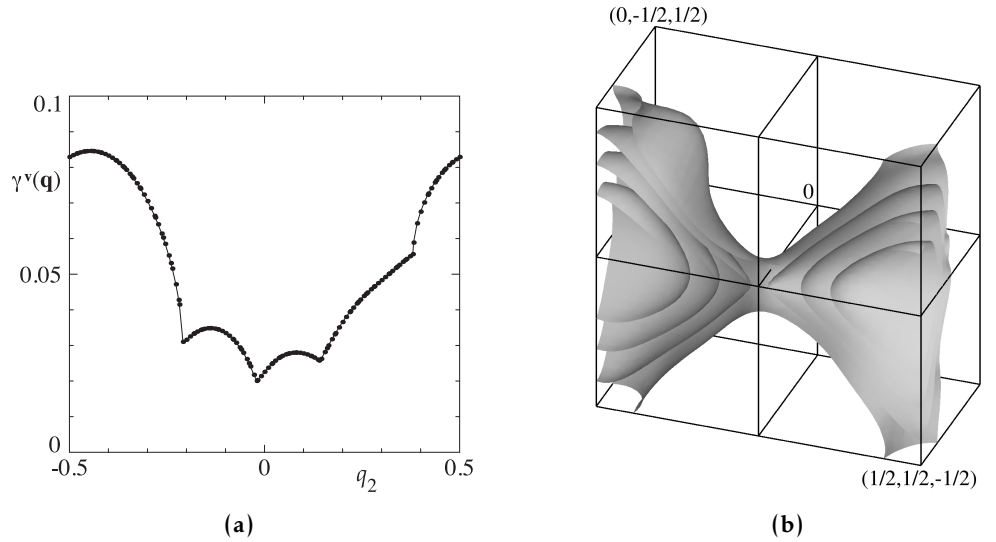

Figure 8. For $\nu = 0.1$, dominant growth rates $\gamma^{\mathbf{v}}(\mathbf{q})$ of the Bloch hydrodynamic stability modes as a function of q_2 on the line $q_1 = 0.34$, $q_3 = -0.36$ (a), isosurfaces of the growth rates at the levels of 60%, 70%, 80% and 90% of the maximum over $\mathbb{Q}$ growth rate $\gamma^{\mathbf{v}}(\mathbf{q}) = 0.1356$ for $\mathbf{q} = (1/2, -1/2, 0)$ (b) for a sample parity-invariant steady flow of type E. The axis q_1 points towards the reader, the frontal vertical plane is $q_1 = 1/2$, the q_2 axis points to the right, and the q_3 axis is vertical.

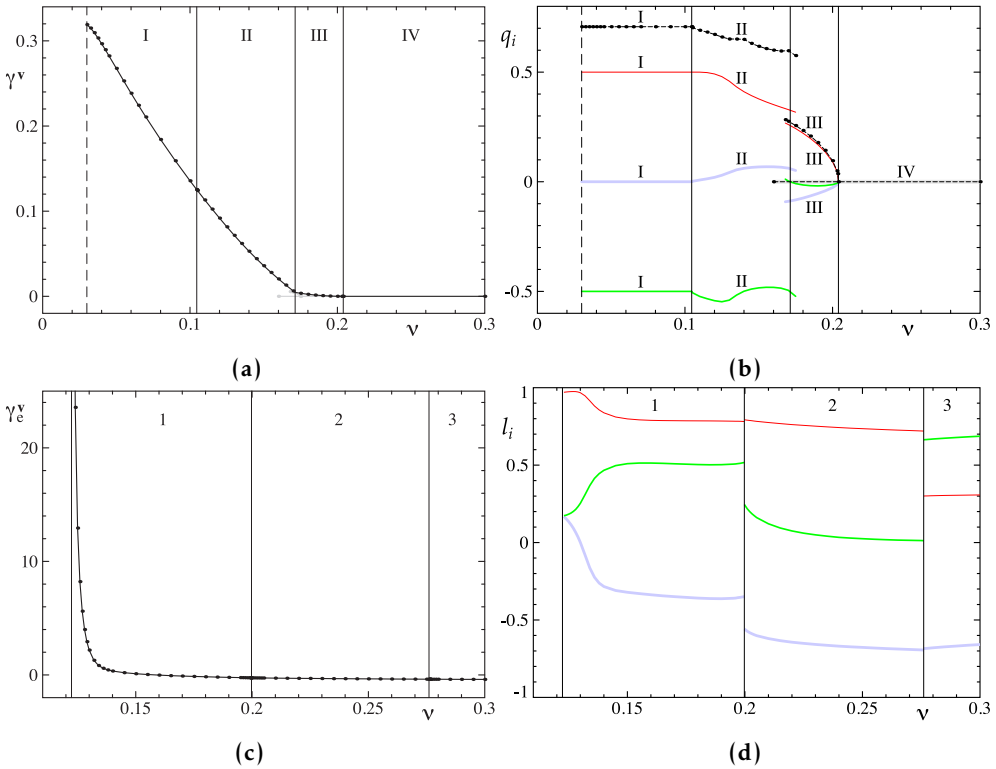

Figure 9. Same as Figure 6, but for the sample parity-invariant steady flow of type E. The growth rates in interval I are globally maximum over $\mathbb{Q}$ for $\mathbf{q} = (1/2, -1/2, 0)$, and $\gamma^{\mathbf{v}}(\mathbf{q}) = 0$ for $\mathbf{q} = 0$ is globally maximum in interval IV.

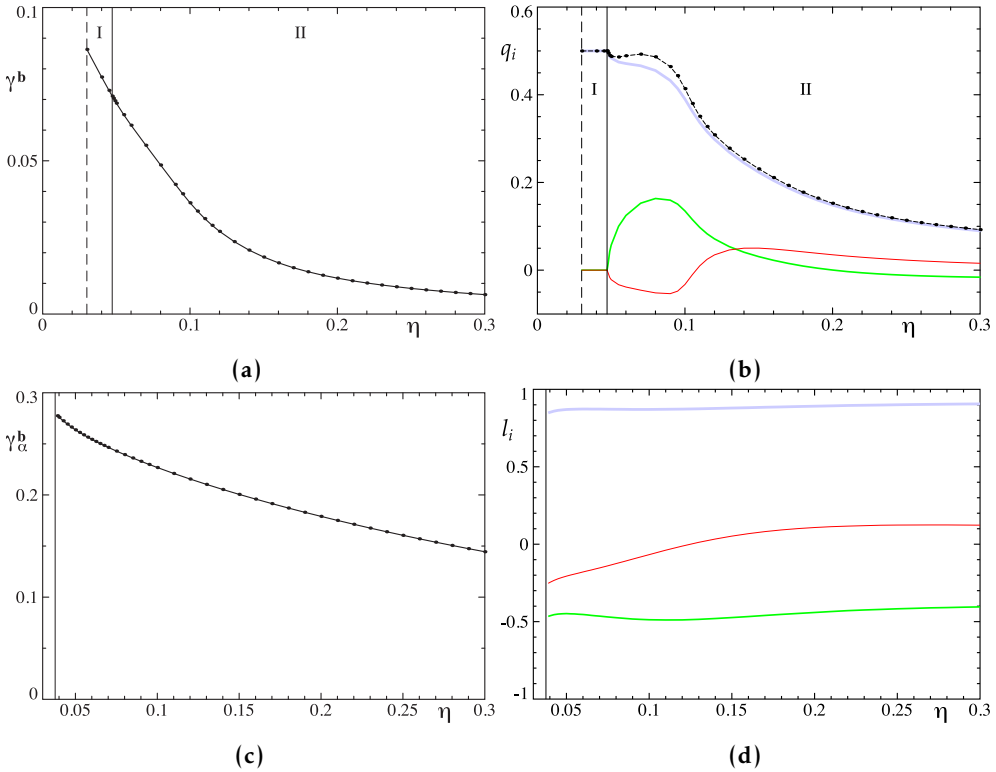

Figure 10. Maximum growth rates of the Bloch magnetic modes (a) and maximum slow-time growth rates due to the action of the magnetic α-effect (c) for a sample non-parity-invariant steady flow of type V. Wave vectors $\mathbf{q}$ (b), for which the growth rates are shown in (a), and directions of the wave vectors (d), for which the growth rates are shown in (c).

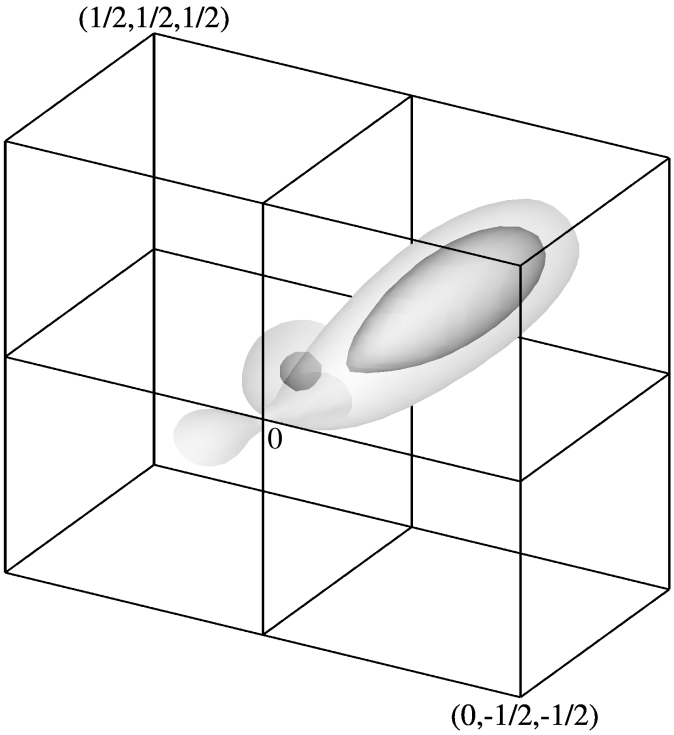

Figure 11. For $\eta = 0.1$, isosurfaces of the dominant growth rates $\gamma^{\mathbf{b}}(\mathbf{q})$ at the levels 0 and a half of the maximum over $\mathbb{Q}$ growth rate (the internal darker structures) for a sample non-parity-invariant steady flow of type I. The maximum over $\mathbb{Q}$ value $\gamma^{\mathbf{b}}(\mathbf{q}) = 0.0097$ is located at $\mathbf{q} = (0.3333, -0.1805, 0.1742)$. The axis q_1 points inside $\mathbb{Q}$, the q_2 axis to the left, and the q_3 axis is vertical.

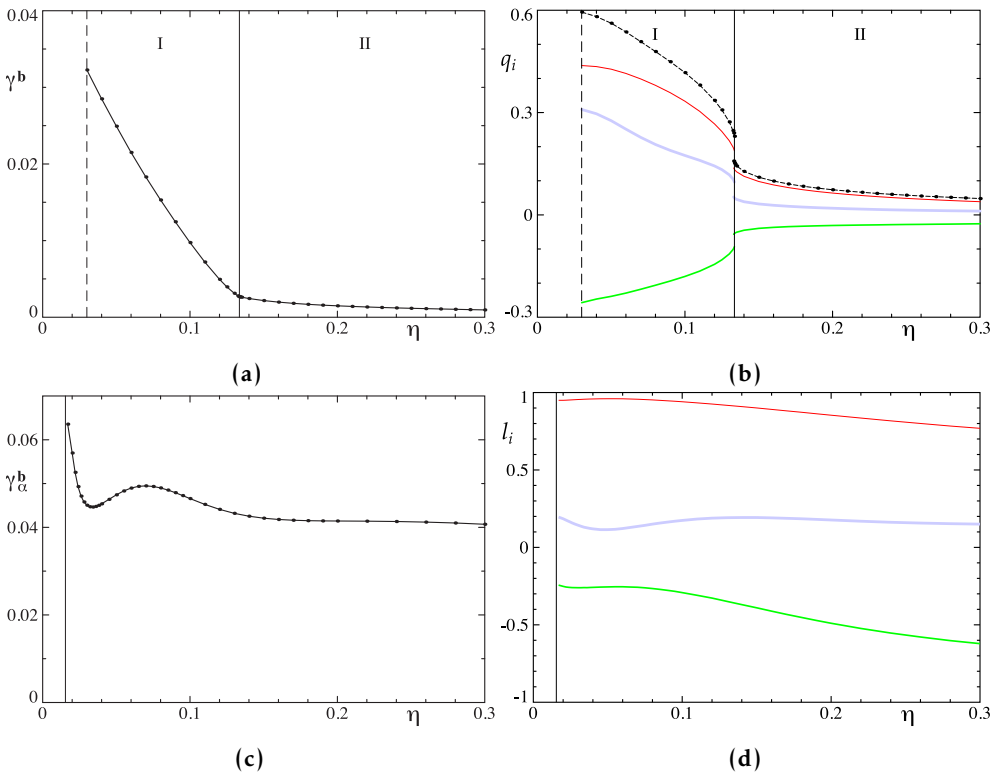

Figure 12. Same as Figure 10, but for the sample non-parity-invariant steady flow of type I.

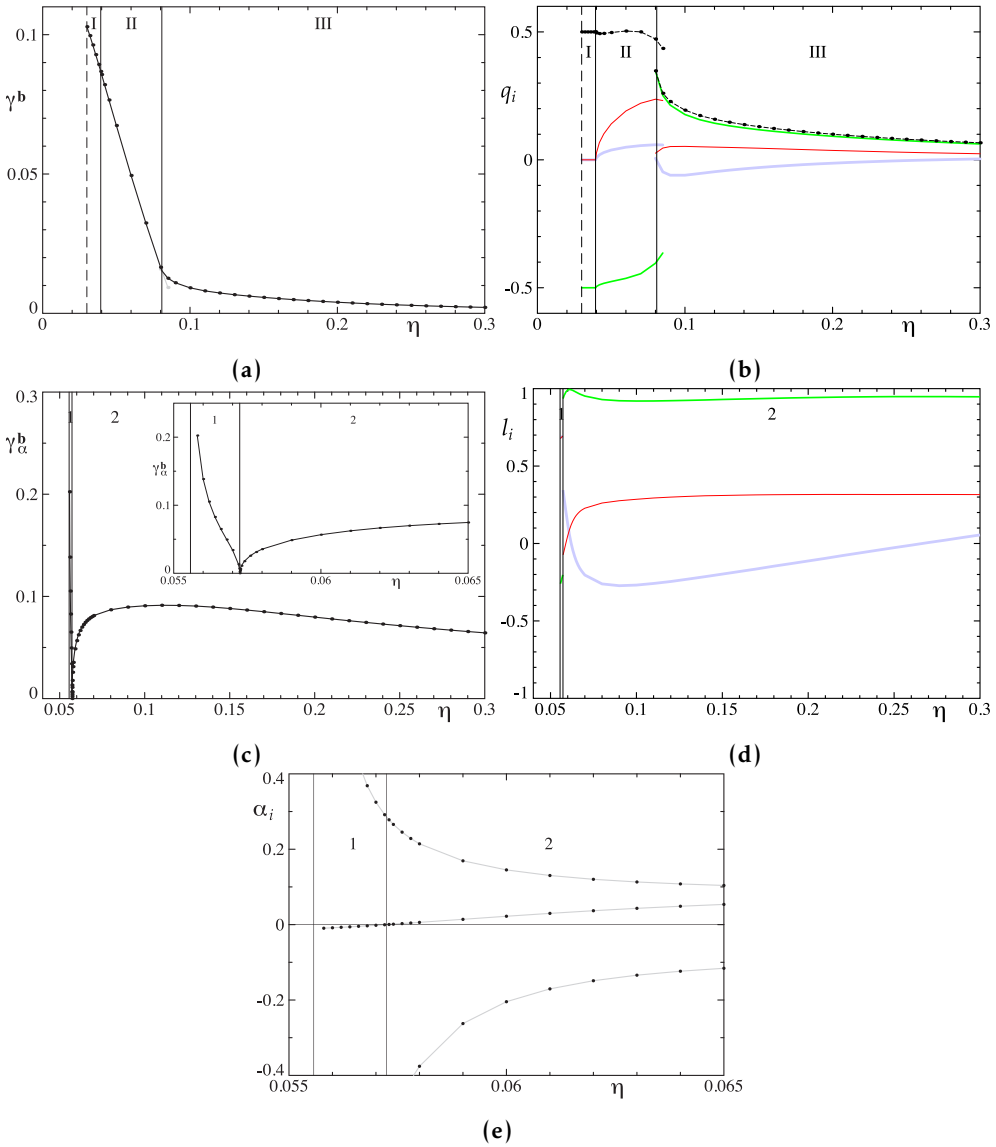

Figure 13. Panels (a)–(d) same as (a)–(d) in Figure 10, but for a sample non-parity-invariant steady flow of type E. In interval I, the growth rates are globally maximum over $\mathbb{Q}$ for $\mathbf{q} = (0, -1/2, 0)$. Eigenvalues of the symmetrized α-effect tensor (e). The insert in (c): a zoom of the plot (c) near the point of singular behavior of $\gamma^{\mathbf{b}}_\alpha$. The cusp is located at η (shown by the right thin vertical line in (c) and (e)), for which the intermediate eigenvalue of the symmetrized α-effect tensor vanishes.

encounter the instance of $q_1 = q_2 = q_3 = 1/2$ in the kinematic dynamo problem for a sample parity-invariant flow of type E (Figure 16), but usually such case is $\mathbf{q} = 0$. In this connection we recall that there always exist neutral (i.e., such that $\lambda(\mathbf{q}) = 0$) perturbation modes for $\mathbf{q} = 0$; they have globally maximum growth rates for sufficiently large ν or η (see also a discussion at the end of section 5 of [*Chertovskih and Zheligovsky*, 2023]).

The plots in panels (b) reveal, that typically the wave vectors $\mathbf{q}$, for which the growth rates are globally maximum, suffer discontinuity at the boundaries of the intervals of dominance, i.e., the branches are independent. A notable exception, encountered when computing perturbation modes of parity-invariant flows or MHD states, is branches bifurcating from branches of Bloch modes for half-integer wave vectors $\mathbf{q}$ (see, e.g., Figures 6, 9, 14, 15, 21 and 22). A formal asymptotic expansion of the offshoots stemming from a branch for $\mathbf{q} = 0$ in the kinematic dynamo problem will be constructed in the next paper of this series. Continuing a branch outside its interval of dominance is not always possible, e.g., continuation of branches I into regions II fails in the dynamo problem for the sample flows

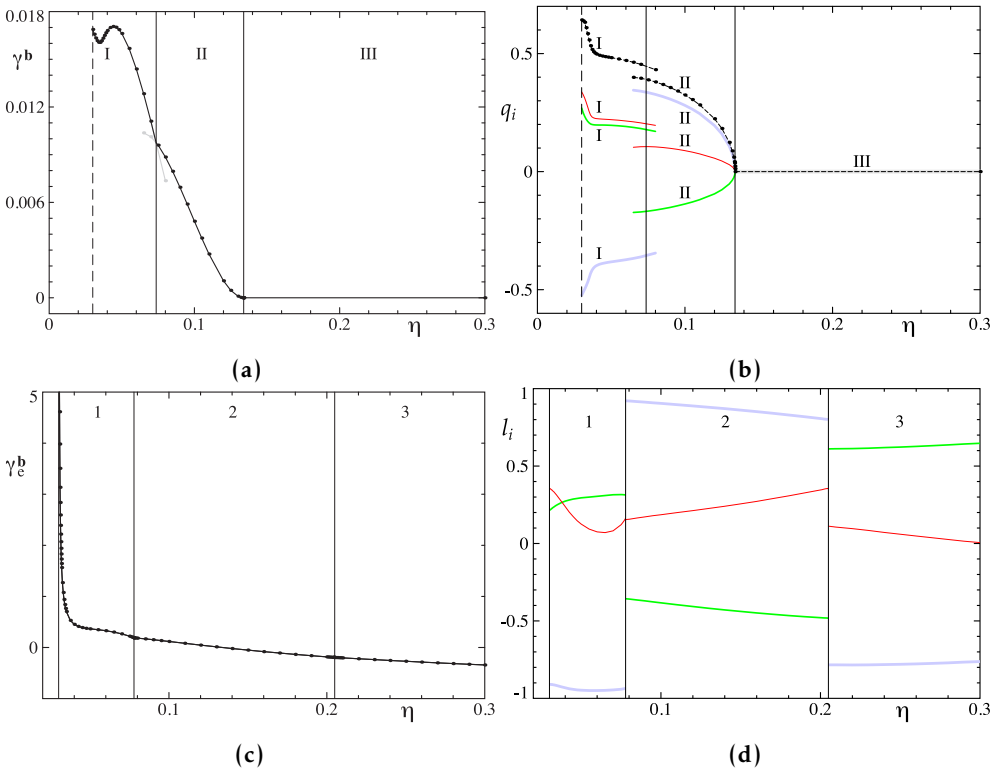

Figure 14. Panels (a), (b) and (d) same as in Figure 10a, 10b and 10d, but for a sample parity-invariant steady flow of type V, and maximum slow-time growth rates due to the action of the magnetic eddy diffusivity Figure 10c. In interval III, the growth rate $\gamma^{\mathbf{b}}(\mathbf{q}) = 0$ for $\mathbf{q} = 0$ is globally maximum over $\mathbb{Q}$.

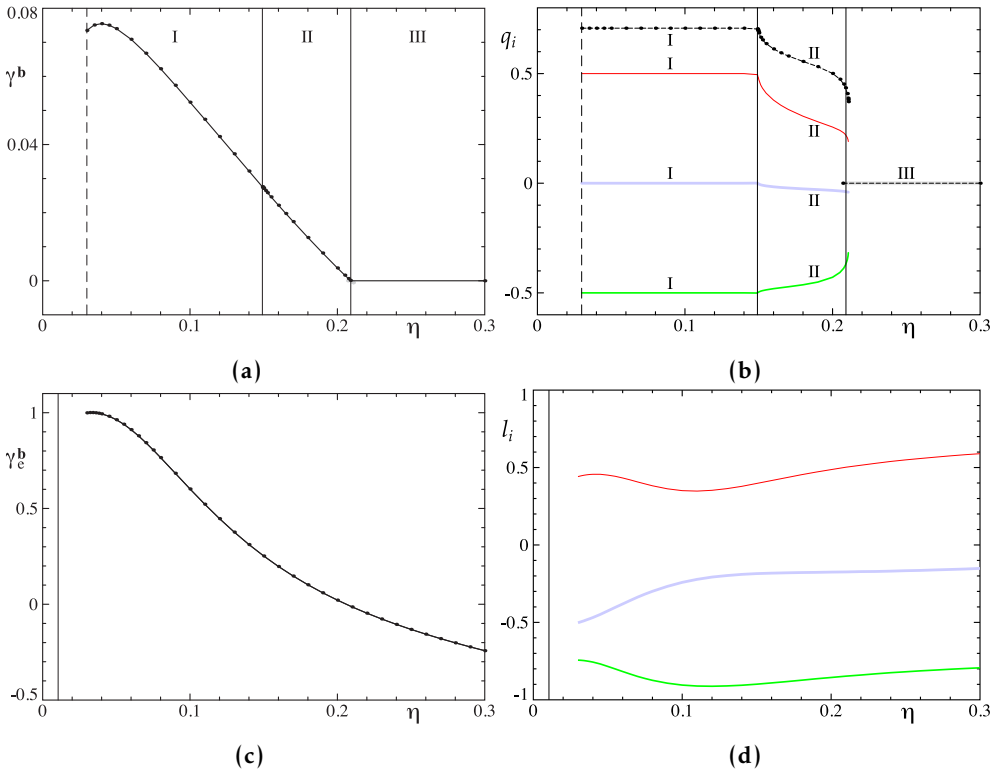

Figure 15. Same as in Figure 14, but for a sample parity-invariant steady flow of type I. In interval I, the growth rates are globally maximum over $\mathbb{Q}$ for $\mathbf{q} = (1/2, -1/2, 0)$, and $\gamma^{\mathbf{b}}(\mathbf{q}) = 0$ for $\mathbf{q} = 0$ is globally maximum in interval III.

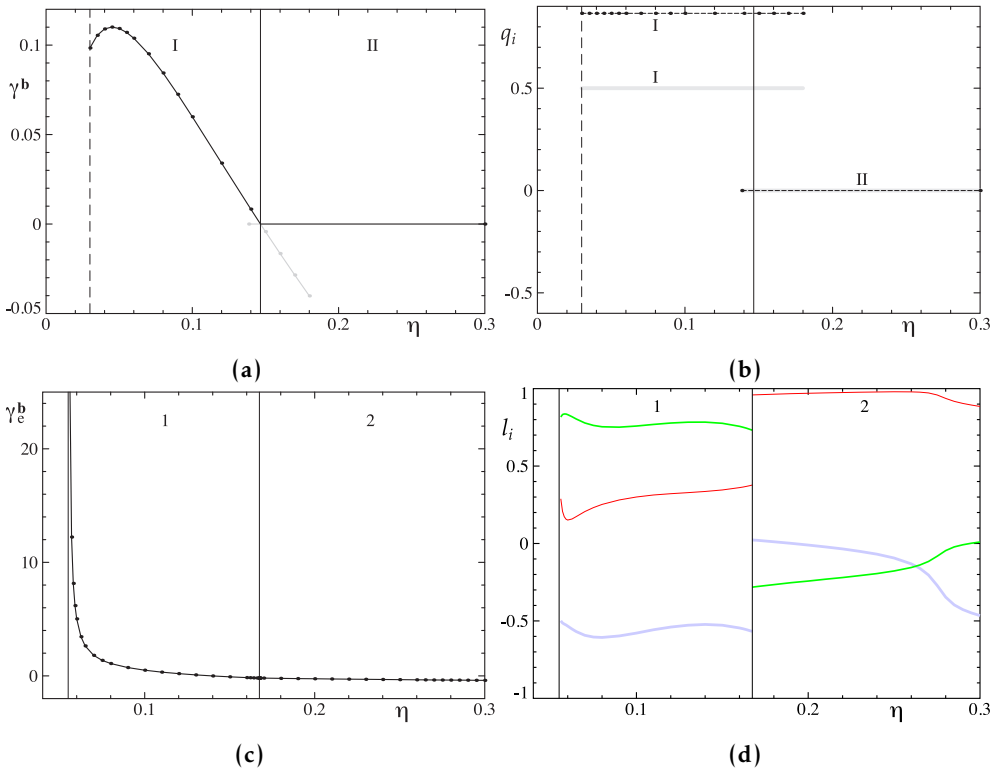

Figure 16. Same as in Figure 14, but for a sample parity-invariant steady flow of type E. In intervals I and II, the growth rates are globally maximum over $\mathbb{Q}$ for $\mathbf{q} = (1/2, 1/2, 1/2)$ and $\mathbf{q} = 0$, respectively.

of types V and E possessing the magnetic α-effect (Figures 10 and 13), because in regions II continuations of the branches I do not consist of locally maximum growth rates (the Hessians of the growth rates are not sign-defined). This suggests that for the two samples the branches II bifurcate from branches I and have the asymptotics similar to the one for offshoots bifurcating from branches for $\mathbf{q} = 0$.

Figures 3, 5, 8, 11 and 17 display isosurfaces of the dominant growth rate (i.e., the largest real part of all eigenvalues of the stability operator) in the domain $\mathbb{Q}$. To construct the isosurfaces, we have computed the dominant growth rates on uniform meshes comprised of $25 \times 50 \times 50$ mesh points for Figures 3, 5, 8, or $20 \times 40 \times 40$ mesh points for Figures 11 and 17. The presence of at least 4 local maxima is observed in Figure 3b, 6 in Figure 5b, just 1 in Figure 8b, 2 in Figure 11 and 4 in Figure 17b. The complexity of the dependence of the dominant growth rate on the wave vector $\mathbf{q}$ is also illustrated by the plot of its isolines in a cross-section of $\mathbb{Q}$ in Figure 3a. Graphs reveal 3 regions of smooth behavior of the dominant growth rate on varying q_2 along the line $q_1 = 0.48$, $q_3 = 0.3$ (Figure 3a), 4 regions along the line $q_1 = 0.44$, $q_3 = 0.16$ (Figure 5a), 4 regions along the line $q_1 = 0.34$, $q_3 = -0.36$ (Figure 8a) and 3 regions along the line $q_1 = 0.2$, $q_3 = -0.15$ (Figure 17a). The presence of several local maxima in $\mathbb{Q}$ and the loss of smoothness on the boundaries between branches of dominant stability modes implies that solving the system of equations $\partial\gamma/\partial q_m = 0$ is not an optimal numerical strategy for finding the globally (in the domain $\mathbb{Q}$) maximum growth rate.

Like the growth rates of the Bloch modes, the maximum slow-time growth rates due to the action of the α-effect or eddy diffusivity depend continuously on ν or η and constitute branches, in which the dependencies of the growth rate and the direction $\mathbf{l}$ of the wave vector $\mathbf{q} = \varepsilon\mathbf{l}$, for which the growth rate is maximum, on the molecular diffusivity parameter are smooth. We assign the name "the interval of dominance of a branch" to the interval, where the growth rates of modes constituting the branch are globally maximum. In plots of maximum slow-time growth rates (panels (c) and (d) in Figures 1–23 except Figures 3, 5, 8, 11, 17), intervals of dominance of individual branches are demarcated by thin

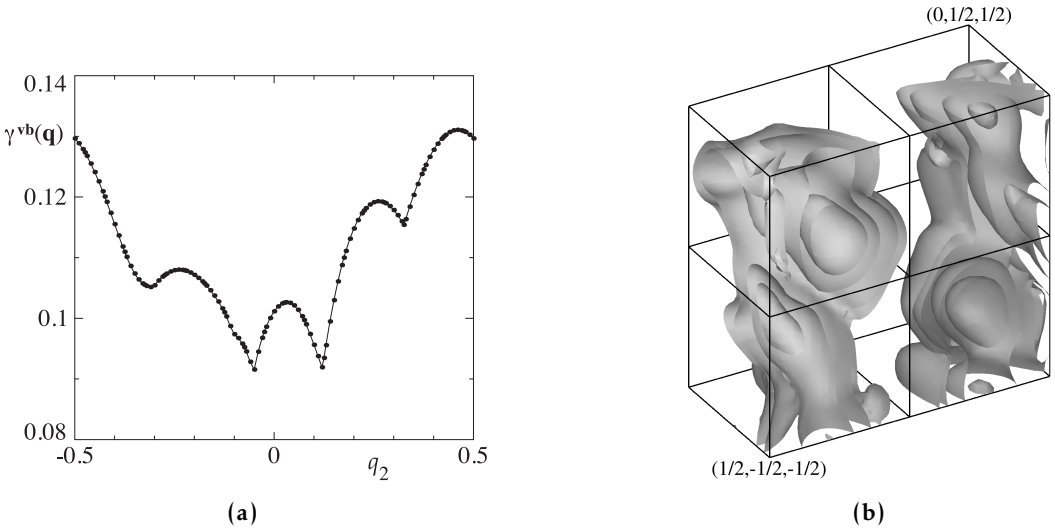

Figure 17. For $\nu = \eta = 0.1$, dominant growth rates $\gamma^{\mathbf{vb}}(\mathbf{q})$ of the Bloch MHD stability modes as a function of q_2 on the line $q_1 = 0.2$, $q_3 = -0.15$ (a) and isosurfaces of the growth rates for a sample non-parity-invariant MHD steady state of type V shown in $\mathbb{Q}$ at the levels of 75%, 80%, 90% and 95% of the maximum over $\mathbb{Q}$ value $\gamma^{\mathbf{vb}}(\mathbf{q}) = 0.1762$ (b) for $\mathbf{q} = (0.4888, 0.2536, -0.2075)$. The axis q_1 points towards the reader, the frontal vertical plane is $q_1 = 1/2$, the q_2 axis points to the right, and the q_3 axis is vertical.

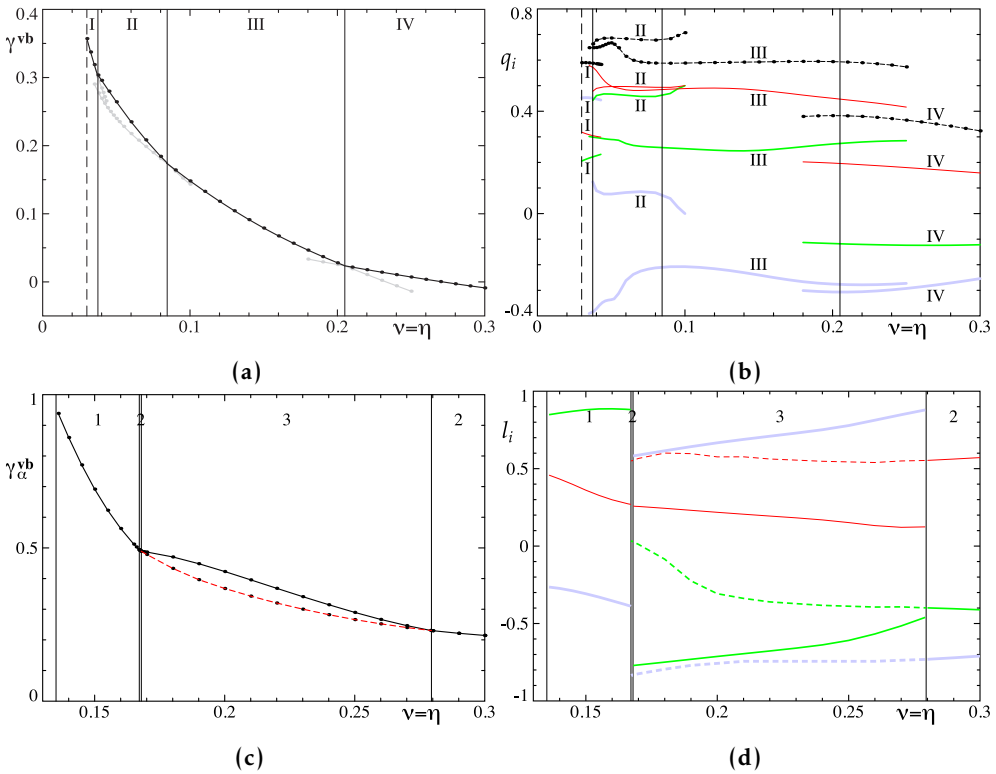

Figure 18. Maximum growth rates of the Bloch MHD linear stability modes (a) and maximum slow-time growth rates due to the action of the combined MHD α-effect (c) for the sample non-parity-invariant MHD steady state of type V, for $\nu = \eta$. Wave vectors $\mathbf{q}$ (b), for which the growth rates are shown in (a), and directions of the wave vectors (d), for which the growth rates are shown in (c). Slow-time growth rates of large-scale MHD stability modes constituting branch 2 are globally maximum in two disjoint intervals of $\nu = \eta$; in the intervening interval of dominance of branch 3, branch 2 and the respective components of the wave vectors $\mathbf{q}$ are shown by dashed lines in (c), (d).

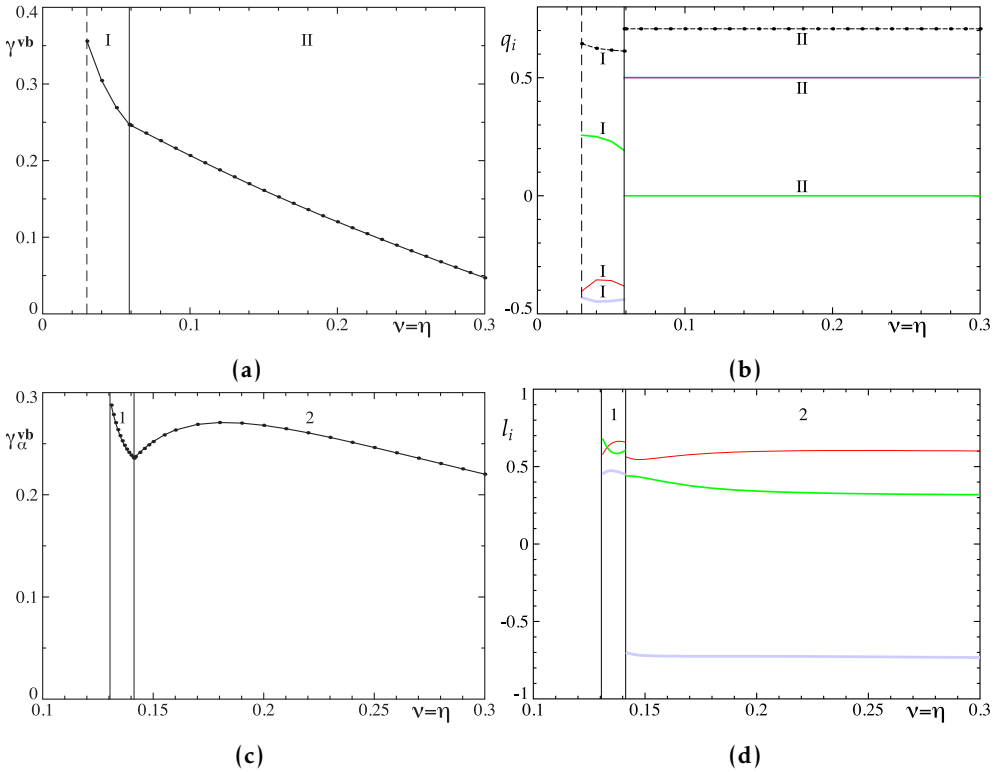

Figure 19. Same as in Figure 18, but for a sample MHD non-parity-invariant state of type I. In interval II, the growth rates are globally maximum over $\mathbb{Q}$ for $\mathbf{q} = (1/2, 0, 1/2)$.

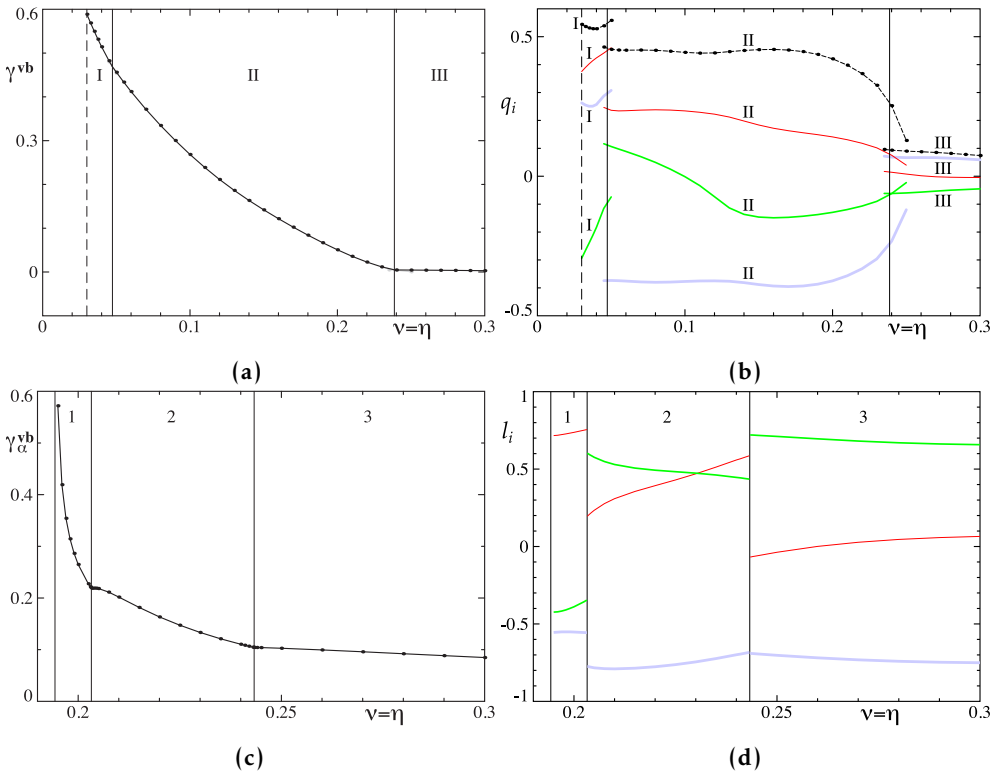

Figure 20. Same as in Figure 18, but for a sample non-parity-invariant MHD state of type E.

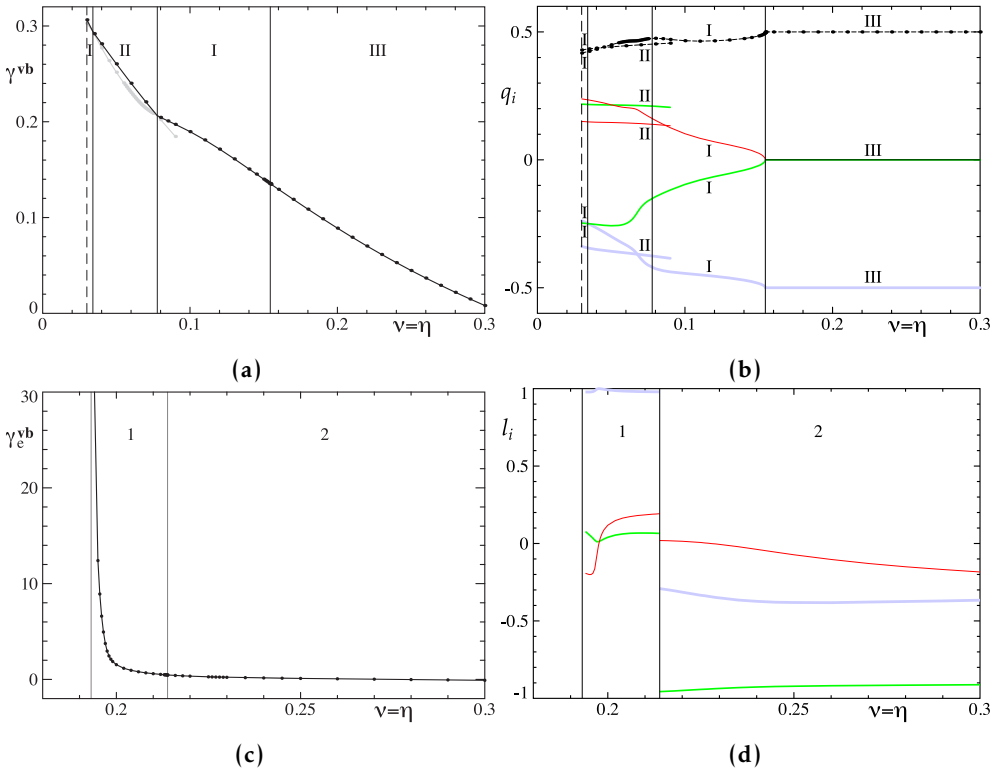

Figure 21. Panels (a), (b) and (d) same as in Figure 18a, 18b and 18d, but for a sample parity-invariant steady MHD state of type V, and maximum slow-time growth rates due to the action of the magnetic eddy diffusivity Figure 18c. In interval III, the growth rates are globally maximum over $\mathbb{Q}$ for $\mathbf{q} = (0, 0, -1/2)$. Growth rates of the Bloch MHD stability modes constituting branch I are globally maximum in two disjoint intervals of $\nu = \eta$ (a), (b).

vertical lines and numbered by arabic numbers. The number of the detected independent intervals of dominance of branches of slow-time growth rates due to the action of the α-effects (eddy diffusivities) varies in our computations for different problems from 1 to 4 (from 1 to 3, respectively). Like in the case of branches of growth rates of the Bloch instability modes, branches can often be extended outside their intervals of dominance into branches of local, but not global maximum slow-time growth rates. We have not performed such continuations (with the exception of Figure 18). In panels (d), red, green and blue lines show the components l_i of the unit vector $\mathbf{l}$ in the direction of the wave vector $\mathbf{q}$ for which the slow-time growth rate is maximum.

Computations of large-scale MHD stability modes for the sample MHD steady state of type V have revealed an unusual phenomenon: Slow-time growth rates of large-scale MHD stability modes due to the action of the combined MHD α-effect, constituting branch 2, are globally maximum in two disjoint intervals of $\nu = \eta$ (in the intervening interval of dominance of branch 3, branch 2 and the respective components of the wave vectors $\mathbf{q}$ are shown by dashed lines in Figure 18c, 18d). Similarly, for the sample parity-invariant MHD states of types V and E, growth rates of the Bloch MHD stability modes constituting branch I (III, respectively) turn out to be globally maximum in two disjoint intervals of $\nu = \eta$ (Figures 21a, 21b and 23a, 23b). The branch III in Figure 23a, 23b is also notable in that it both begins and ends in bifurcations of two branches for $\mathbf{q} = 0$ (the globally maximum growth rate is $\gamma^{\mathbf{vb}}(\mathbf{q}) = 0$ in the left, and the short-scale eigenmodes are unique and have strictly positive growth rates in the right).

The horizontal axes in panels (c) and (d), showing maximum slow-time growth rates due to the action of the α-effect or eddy diffusivity, are typically chopped off in the left and do not span the complete intervals $0.03 \le \nu, \eta \le 0.3$, for which we have done computations. The reason is that the slow-time growth rates have vertical asymptotes at the critical values

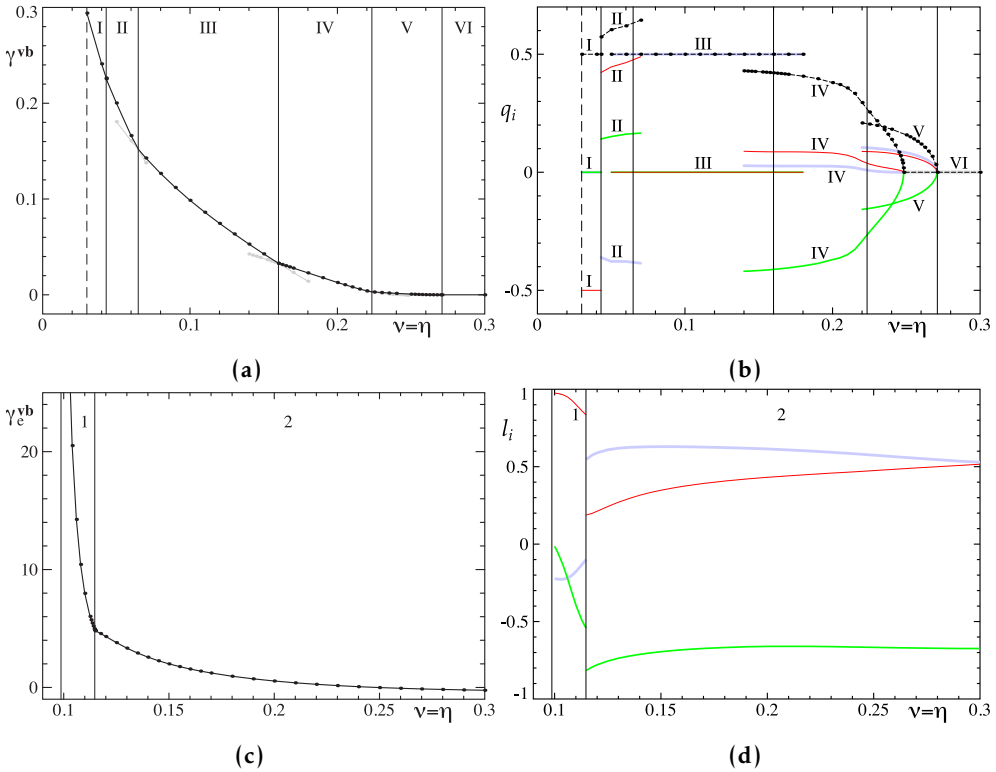

Figure 22. Same as in Figure 21, but for a sample parity-invariant steady MHD state of type I. In intervals I and III, the growth rates are globally maximum over $\mathbb{Q}$ for $\mathbf{q} = (-1/2, 0, 0)$ and $\mathbf{q} = (0, 0, 1/2)$, respectively, and in interval IV $\gamma^{\mathbf{vb}}(\mathbf{q}) = 0$ for $\mathbf{q} = 0$ is globally maximum.

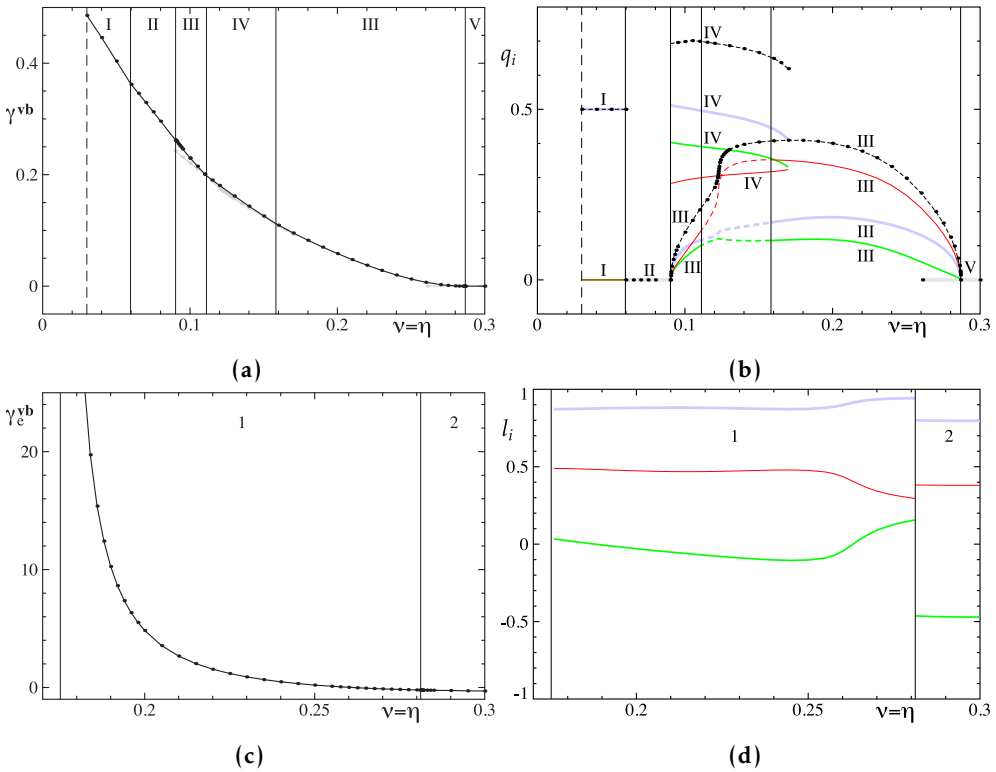

Figure 23. Same as in Figure 21, but for a sample parity-invariant MHD state of type E. In interval I, the growth rates are globally maximum over $\mathbb{Q}$ for $\mathbf{q} = (0, 0, 1/2)$, and in intervals II and V for $\mathbf{q} = 0$ ($\gamma^{\mathbf{vb}}(\mathbf{q}) = 0$ in interval V).

of the diffusivity parameters ν or η, at which the monotonic small-scale instability sets in (the hydrodynamic or MHD instability, or the dynamo action, depending on the problem at hand), i.e., at which the eigenvalue associated with the dominant small-scale (for $\mathbf{q} = 0$) zero-mean mode of the linearization vanishes (on decreasing from the parameter values for which the flow or MHD state is stable). This phenomenon does not occur for the oscillatory loss of stability, when the respective eigenvalue is imaginary. It was described in *Zheligovsky* [2011] for the eddy diffusivity and discovered in *Rasskazov et al.* [2018] for the magnetic α-effect; the same arguments explain a similar asymptotics for the AKA and combined MHD α-effects. The vertical asymptotes for the slow-time instability growth rates due to the action of the α-effects or eddy diffusivities are shown in panels (c) and (d) by the left thin vertical lines, located at the critical points of the onset of the short-scale instability.

As discussed in section 5.1 of [*Chertovskih and Zheligovsky*, 2023], the kinematic dynamo problem is specific in that the maximum slow-time growth rate $\gamma_\alpha^{\mathbf{b}}$ due to the action of the magnetic α-effect is determined in terms of the eigenvalues α_i of the symmetrized magnetic α-effect tensor ${}^{\mathrm{s}}\mathbf{A}^{\mathbf{bb}} = (\mathbf{A}^{\mathbf{bb}} + (\mathbf{A}^{\mathbf{bb}})^*)/2$:

$$\gamma_\alpha^{\mathbf{b}} \equiv \max_{\theta,\varphi} \operatorname{Re} \lambda_1^{\mathbf{b}}(\theta,\varphi) = \sqrt{\max(\alpha_1\alpha_2, \alpha_2\alpha_3, \alpha_1\alpha_3)}$$

(see [*Rasskazov et al.*, 2018]). This implies that $\gamma_\alpha^{\mathbf{b}} = 0$ only for such molecular diffusivity η_*, that the intermediate in value eigenvalue of ${}^{\mathrm{s}}\mathbf{A}^{\mathbf{bb}}$ vanishes (generically the three eigenvalues are distinct), and then $\gamma_\alpha^{\mathbf{b}} = \mathrm{O}(|\eta - \eta_*|^{1/2})$. We encounter this phenomenon for a non-parity-invariant sample flow of type E (see Figure 13). The insert in panel (c) shows a zoom of the plot of $\gamma_\alpha^{\mathbf{b}}$ near the point η_* at which $\alpha_2 = 0$ (see Figure 13e); it has the form of a cusp agreeing with the asymptotics $\gamma_\alpha^{\mathbf{b}} = \mathrm{O}(|\eta - \eta_*|^{1/2})$.

4. Conclusions

We have addressed the following question: Suppose a flow or an MHD state characterized by a significant separation of scales has emerged. Will the scale separation persist during the subsequent evolution of the flow and magnetic field? As it turns out, the answer is negative: it is likely to be destroyed by the instability to perturbations of the spatial scale that is slightly larger than that of the flow or MHD state experiencing a perturbation.

In agreement with [*Zheligovsky and Chertovskih*, 2020], our numerical results demonstrate that, at least in the limited interval of the molecular diffusivity parameters values for which we have performed computations of the Bloch eigenmodes, the three linear stability problems under consideration: the kinematic dynamo problem, the hydrodynamic and MHD stability problems – show a remarkably similar behavior, irrespective of the energy spectrum of the steady flow and magnetic field $(\mathbf{V}, \mathbf{B})$ subjected to perturbation. For generic steady flows and MHD states, the Bloch modes, that have the maximum over $\mathbf{q}$ growth rates, feature spatial scale separation that enhances on increasing the diffusivity ν and/or η. The length of the wave vector $\mathbf{q}$, for which the growth rate is maximum, is between 0.36 (Figure 1) and 0.71 (Figure 2) for the smallest considered $\nu, \eta = 0.03$, and it decreases to the values between 0.01 (Figure 2) and 0.32 (Figure 18) for the largest considered $\nu, \eta = 0.3$. (We recall that a small positive $|\mathbf{q}|$ manifests high scale separation, but no scale separation is present for $\mathbf{q} = 0$.) Most instability modes for parity-invariant steady flows or MHD states also share this property: the length of $\mathbf{q}$ maximizing the growth rate is in the range between 0.43 (Figure 7) and $\sqrt{3/4}$ (Figure 16) for $\nu, \eta = 0.03$, and it decreases to the values between 0 (e.g., Figures 14–16) and 0.20 (Figure 6) for $\nu, \eta = 0.3$.

A physical explanation is straightforward: the larger the diffusivities, the more stabilizing the effect of diffusion is at a given spatial scale relative the destabilizing effect of advection (since diffusion, described by a second-order partial differential operator, competes with advection, described by a first-order operator); therefore, for a higher diffusivity, instability is more efficient at larger space scales. However, instability due to the α-effects (growth rates order the scale ratio, when it is small) or eddy diffusivity/viscosity (growth rates order the scale ratio squared), emerging at a high scale separation, remain "invisible",

being overshadowed by a faster (growth rates order unity) growing instability modes featuring a modest scale separation. Of course, this argument is only heuristic; in fact, the opposite occurs for one non-parity-invariant ($|\mathbf{q}|$ grows from 0.65 for $\nu = \eta = 0.03$ to $\sqrt{1/2}$ for $\nu = \eta = 0.3$, Figure 19) and one parity-invariant ($|\mathbf{q}|$ grows from 0.45 for $\nu = \eta = 0.03$ to $1/2$ for $\nu = \eta = 0.3$, Figure 21) MHD state. Also, it does not explain why the growth rates have maxima inside intervals of dominance, e.g., I in Figures 1, 2, 4 for non-parity-invariant flows, or III in Figures 7 and 9, and II in Figure 22 for parity-invariant steady states.

The details of the behavior may differ: the overall decrease of growth rates on increasing the diffusivity parameter can be monotonic or non-monotonic, their maxima over wave vectors of the Bloch amplitude modulation can be continuous or discontinuous, and the intervals of their continuity can split into several intervals of smooth dependence. The behavior of the maximum growth rates as functions of the diffusivity parameters appears completely independent of the behavior of the slow-time growth rates due to the action of an α-effect or eddy diffusivity/viscosity; this can be expected, since the two growth rates are determined as solutions to algebraically different problems.

Magnetic α-effect is at present widely used for explaining the origin of astrophysical magnetic fields, in particular, of the solar and geomagnetic fields. Eddy ("turbulent") diffusivity is also theoretically important: it is believed that it is responsible for the similarity of many numerical geodynamo models despite the rheological parameter values used were by orders of magnitude more computationally favorable than those characterizing the conditions of the Earth's outer core (see, e.g., [*Starchenko*, 2017]). Our results suggest that the α-effect and eddy diffusivity that are based on spatial scale separation are not reliable dynamo mechanisms in this context. Any given scale range, sufficiently small compared to the size of the fluid container, gives rise to perturbations involving somewhat larger, but not significantly larger spatial scales. Thus, the full evolution consists of a cascade of instabilities each generating a not-very-much-larger scale. It creates flows and magnetic fields that lack high scale separation and occupy all available spatial scale slots; if at a certain time a significant separation of spatial scales emerges, the cascade destroys it. It is doubtful that such a highly nonlinear cascade can be described by a differential operator of a simple structure, such as the operators of the α-effect or eddy diffusivity.

The expected cascade of instabilities giving rise to additional spatial frequencies is reminiscent of the L. D. Landau scenario of development of turbulence [*Landau and Lifshitz*, 1987], in which flow gradually becomes more and more complex as a result of appearance, in a sequence of bifurcations, of temporal frequencies that are incommensurable with those already present in the flow. However, there exists a profound difference between the theories of the α-effect and hydrodynamic turbulence. Although the laws of hydrodynamic turbulence have not been derived from the first principles without additional assumptions originating in physics, they have a firm foundation in the vast body of data accumulated in experiments, for instance, in wind tunnels. By contrast, to the best of our knowledge, just a single experiment [*Steenbeck et al.*, 1968] was conducted to detect the emergence of the magnetic α-effect. Thus, the familiar mathematical expression for the α-effect has been rigorously derived only for the case of asymptotically high scale separation (see the discussion and references in [*Chertovskih and Zheligovsky*, 2023]), and it is desirable to establish the general laws describing the influence of small-scale magnetic and fluid structures on large-scale ones. A similar problem of quantifying the influence of the subgrid-scale structures on the evolution of the larger-scale structures arises in the context of the Large Eddy Simulation (LES) numerical methods.

Other mechanisms for formation of the α-effect have been considered in the literature, e.g., the α-effect in an almost axisymmetric fluid flow, or in turbulence, whose origin is of a statistical nature and results from ensemble averaging. The magnetic α-effect of [*Braginsky*, 1964a,b] in a weakly non-axisymmetric flow is advantageous in that it is not affected by the mechanism that erodes the α-effect relying on high spatial scale separation: Existence of the Braginskii α-effect was demonstrated in cylindrical coordinates by averaging in the azimuthal variable ϕ. By analogy with the scale separation in Cartesian

variables investigated here, it is algebraically possible to consider "Bloch modes" of the form $e^{ßq\phi}\mathbf{b}(\mathbf{x})$, but they are geometrically inconsistent unless q is integer. It remains to be investigated how our results and conclusions are modified when the underlying flows and steady states are non-periodic.

Finally, let us note that the inefficiency of the magnetic α-effect relying on scale separation in Cartesian variables examined here appears to abate the importance of the phenomenon of α-quenching [*Vainshtein and Cattaneo*, 1992].

Acknowledgments

The project was financed by the grant No. 22-17-00114 of the Russian Science Foundation, https://rscf.ru/project/22-17-00114/. A part of computations was carried out on the OBLIVION Supercomputer at the University of Évora, Portugal (the FCT advanced computing project 2021.09815.CPCA).

References

Braginsky, S. I. (1964a), Self-excitation of a magnetic field during the motion of a highly conducting fluid, *Soviet Physics JETP*, *20*, 726–735 (in Russian).

Braginsky, S. I. (1964b), Theory of the hydromagnetic dynamo, *Soviet Physics JETP*, *20*, 1462–1471 (in Russian).

Chertovskih, R., and V. Zheligovsky (2023), Linear perturbations of the Bloch type of space-periodic magnetohydrodynamic steady states. I. Mathematical preliminaries, *Russian Journal of Earth Sciences*, *23*, ES3001, https://doi.org/10.2205/2023ES000834.

Frisch, U. (1995), *Turbulence: The legacy of A. N. Kolmogorov*, Cambridge University Press, https://doi.org/10.1017/CBO9781139170666.

Krause, F., and K.-H. Radler (1980), *Mean-Field Magnetohydrodynamics and Dynamo Theory*, Elsevier, https://doi.org/10.1016/c2013-0-03269-0.

Landau, L. D., and E. M. Lifshitz (1987), *Fluid Mechanics. Volume 6 of Course of Theoretical Physics*, 2nd ed., Pergamon Press.

Rasskazov, A., R. Chertovskih, and V. Zheligovsky (2018), Magnetic field generation by pointwise zero-helicity three-dimensional steady flow of an incompressible electrically conducting fluid, *Physical Review E*, *97*(4), 043,201, https://doi.org/10.1103/PhysRevE.97.043201.

Starchenko, S. V. (2017), Energy geodynamo parameters compatible with analytical, numerical, paleomagnetic models and observations, *Izvestiya, Physics of the Solid Earth*, *53*(6), 908–921, https://doi.org/10.1134/S1069351317050135.

Steenbeck, M., I. M. Kirko, A. Gailitis, A. P. Klyavinya, F. Krause, I. Y. Laumanis, and O. A. Lielausis (1968), Experimental observation of the electromotive force alongside of an external magnetic field induced by the flow of liquid metal (alpha effect), *Doklady Akademii nauk SSSR*, *180*(2), 326–329 (in Russian).

Vainshtein, S. I., and F. Cattaneo (1992), Nonlinear restrictions on dynamo action, *The Astrophysical Journal*, *393*, 165–171, https://doi.org/10.1086/171494.

Zheligovsky, V. (2011), *Large-Scale Perturbations of Magnetohydrodynamic Regimes: Linear and Weakly Nonlinear Stability Theory*, Springer Berlin Heidelberg, https://doi.org/10.1007/978-3-642-18170-2.

Zheligovsky, V. A. (1993), Numerical solution of the kinematic dynamo problem for Beltrami flows in a sphere, *Journal of Scientific Computing*, *8*(1), 41–68, https://doi.org/10.1007/BF01060831.

Zheligovsky, V. A., and R. A. Chertovskih (2020), On Kinematic Generation of the Magnetic Modes of Bloch Type, *Izvestiya, Physics of the Solid Earth*, *56*(1), 103–116, https://doi.org/10.1134/S1069351320010152.